Journal of Molecular Structure 1093 (2015) 144–149

Contents lists available at ScienceDirect

Journal of Molecular Structure

journal homepage: www.elsevier.com/locate/molstruc

# Crystalline TQPP as p-type semiconductor: X-ray crystallographic investigation, OTFT device, and computational analysis of transport properties

Brigitte Wex [a], Ala'a O. El-Ballouli [b], Antoine Vanvooren [c], Ute Zschieschang [d], Hagen Klauk [d], Jeanette A. Krause [e], Jérôme Cornil [c], Bilal R. Kaafarani [b,*]

[a] Department of Natural Sciences, Lebanese American University, P.O. Box 36, Byblos, Lebanon
[b] Department of Chemistry, American University of Beirut, Beirut 1107-2020, Lebanon
[c] Laboratory for Chemistry of Novel Materials, University of Mons, Mons, Belgium
[d] Max Planck Institute for Solid State Research, Heisenbergstr. 1, 70569 Stuttgart, Germany
[e] Department of Chemistry, University of Cincinnati, 404 Crosley Tower, Cincinnati, OH 45221, USA

## HIGHLIGHTS

- **TQPP** materials with thermal stability up to 370 °C were synthesized.
- **TQPP** and **TQPP-[CH$_3$]$_4$** show interplanar stacking distances of 3.4 Å using X-ray crystallography.
- OTFT field-effect mobilities of $10^{-3}$ cm$^2$/V$^{-1}$ s$^{-1}$ for **TQPP** and $10^{-5}$ cm$^2$/V$^{-1}$ s$^{-1}$ **TQPP-[CH$_3$]$_4$**.
- Modeling confirms higher electronic coupling constants for **TQPP** than **TQPP-[CH$_3$]$_4$**.

## GRAPHICAL ABSTRACT

**TQPP** (**X** = **H**): $\mu = 2.5 \times 10^{-3}$ cm$^2$/V s. **TQPP** (**X** = **CH$_3$**): $\mu = 7 \times 10^{-5}$ cm$^2$/V s.

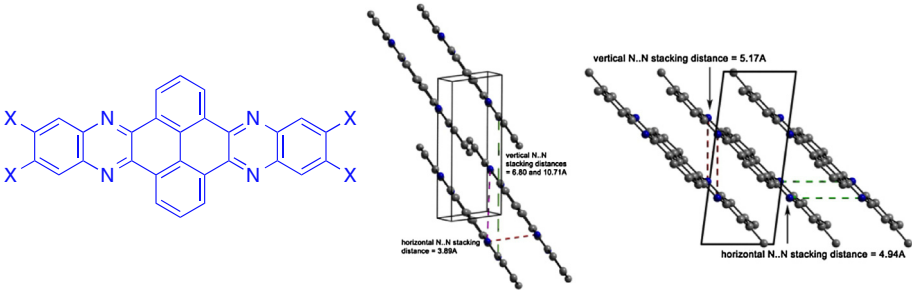


## ARTICLE INFO

*Article history:*
Received 18 January 2015
Received in revised form 24 March 2015
Accepted 25 March 2015
Available online 1 April 2015

*Keywords:*
Azapyrenoacene
Quinoxalinophenanthrophenazine
Organic thin-film transistors
Field-effect mobility
Electronic coupling

## ABSTRACT

Two p-type semiconducting azapyrenoacene materials, quinoxalino[2′,3′:9,10]phenanthro[4,5-*abc*]phenazine (**TQPP**) and 6,7,15,16-tetramethylquinoxalino[2′,3′:9,10]phenanthro[4,5-*abc*]phenazine (**TQPP-[CH$_3$]$_4$**), were characterized and were found to display high thermal stability and planar molecular geometry as revealed by single-crystal X-ray analysis. In bottom-gate p-channel organic thin-film transistors, field-effect mobilities of $2.5 \times 10^{-3}$ cm$^2$/V s and $7.5 \times 10^{-5}$ cm$^2$/V s were measured in ambient air for **TQPP** and **TQPP-[CH$_3$]$_4$**, respectively. Computational results of reorganization energies and electronic couplings indicate larger inter and intra-columnar couplings for **TQPP-[CH$_3$]$_4$** in comparison to **TQPP** and predict the suitability of both semiconductors for hole as well as electron transporters.



## Introduction

Extended, nitrogen-containing heteroacenes are derivatives of extended acene systems and have gained momentum due to their potential toward applications in liquid-crystalline materials [1,2], materials with the ability to self-assemble [3–5], as sensors as well

* Corresponding author. Tel.: +961 3151451.
*E-mail address:* bilal.kaafarani@aub.edu.lb (B.R. Kaafarani).

http://dx.doi.org/10.1016/j.molstruc.2015.03.057
0022-2860/

as dyes [6–9], and as n-type semiconductors [10,11]. The latter aspect was extensively reviewed by Bunz et al. [12–14] and analyzed in a computational study by Winkler and Houk [15]. A sub-class of these materials comprise pyrene-fused pyrazaacenes, as reviewed by Mateo-Alonso, which combine the ease of synthetic versatility, using condensation between tetraketopyrene and diamine of choice, with high thermal stability and interesting materials' properties [16,17]. Alkylthio-substituted pyrene-fused pyraazacenes TQPP-$[SC_{12}H_{25}]_4$ have previously been studied in our group and exhibited saturation hole mobility of $\sim 10^{-3}$ $cm^2$ $V^{-1}$ $s^{-1}$ [18] with a high tilt-angle when compared to the surface normal [19]. In this paper, we apply an efficient synthetic protocol in preparing the electron-deficient discoids, quinoxalino[2′,3′:9,10]phenanthro[4,5-*abc*]phenazine and 6,7,15,16-tetramethylquinoxalino[2′,3′:9,10]phenanthro[4,5-*abc*]phenazine, hereafter referred to as **TQPP** and **TQPP-$[CH_3]_4$**, respectively. Furthermore, we report a combined experimental and theoretical study of exploiting these materials as p-type semiconductors.

## Materials and methods

### *Synthesis*

Tetraketopyrene (**1**) was prepared using a literature procedure [20], diamines **2**, e.g., 1,2-phenylenediamine (**2a**) and 4,5-dimethylphenylenediamine (**2b**) were acquired from commercial sources and used as received.

*General procedure for the synthesis of TQPP-[X]$_4$ (X=H, $CH_3$)*

A solution of 150 mL ethanol: acetic acid (1:1) was added to a mixture of tetraketopyrene **1** (2.67 mmol) and diamine **2** (5.34 mmol), Scheme 1. The reaction mixture was stirred at 120 °C for 24 h, cooled in an ice bath and then filtered to yield a yellow solid. The solid was purified by Soxhlet extraction using toluene and was then recrystallized from 1,2-dichlorobenzene to yield **TQPP-[X]$_4$** (X = H, $CH_3$).

*Quinoxalino[2′,3′:9,10]phenanthro[4,5-abc]phenazine[21] (TQPP)*

Yellow solid. 1.00 g (92%), mp > 300 °C (Lit. >420 °C) [21]. $^1$H NMR (TFA-d, 300 MHz): $\delta$ 10.077 (d, $J$ = 8.1 Hz, 4H), 8.869 (dd, $J_1$ = 6.6 Hz; $J_2$ = 3.3 Hz, 4H), 8.697 (t, $J$ = 8.1 Hz, 2H), 8.499 (dd, $J_1$ = 6.6 Hz; $J_2$ = 3.3 Hz, 4H). $^{13}$C NMR (TFA-d, 75 MHz): $\delta$ 138.329, 137.040, 136.176, 131.335, 130.383, 128.677, 125.198, 124.480 ppm. Anal. Calcd. for $C_{28}H_{14}N_4$: C, 82.74; H,3.47; N, 13.78. Found: C, 82.53; H, 3.29; N, 13.74. MALDI ($m/z$): $[M]^+$ calcd for $C_{28}H_{14}N_4$, 406.12; Found, 406.24.

*6,7,15,16-Tetramethylquinoxalino[2′,3′:9,10]phenanthro[4,5-abc]phenazine (TQPP-$[CH_3]_4$)*

Yellow crystals. 0.75 g (85% yield, mp > 300 °C. $^1$H (TFA-d, 300 MHz): $\delta$ 9.949 (d, $J$ = 8.1 Hz, 4H), 8.619 (t, $J$ = 8.1 Hz, 2H), 8.542 (s, 4H), 2.831 (s, 12H). HRMS-EI ($m/z$): $[M]^+$ calcd for $C_{32}H_{22}N_4$, 462.18445; Found, 462.18232.

### *UV–Vis absorption*

Approx. 1 mg of compound was weighted out and dissolved in spectrophotometry-grade *o*-dichlorobenzene (50 mL) under heating to 70 °C and sonication. Absorbance was recorded in triplicate.

### *Thermal gravimetric analysis (TGA)*

The thermal stability of **TQPP** and **TQPP-$[CH_3]_4$** was probed by thermal gravimetric analysis (TGA) under nitrogen at a heating rate of 2 °C/min. Decomposition temperatures are given as the temperature at which 0.1 wt% loss.

### *Device fabrication*

Bottom-gate, organic thin-film transistors (TFTs) were fabricated using a heavily doped silicon wafer as the substrate and common gate electrode. The silicon surface was thermally oxidized in dry oxygen to obtain a 100-nm-thick layer of silicon dioxide. Onto the $SiO_2$ surface, an 8-nm-thick layer of aluminum oxide was deposited by atomic layer deposition at a substrate temperature of 250 °C. The substrate was then immersed into a 2-propanol solution of tetradecylphosphonic acid (PCI Synthesis) for about 1 h to allow a 1.7-nm-thick self-assembled monolayer (SAM) of the alkylphosphonic acid to form. Thus, the gate dielectric is a combination of 100-nm-thick $SiO_2$, 8-nm-thick $AlO_x$ and a 1.7-nm-thick SAM, having a total thickness of about 110 nm and a capacitance per unit area of 34 nF/$cm^2$. Onto this gate dielectric, a semiconductor layer with a thickness of 30 nm was deposited by sublimation in vacuum. Finally, 30-nm-thick Au source and drain contacts were deposited on top of the semiconductor by thermal evaporation in vacuum through a shadow mask. All TFTs have a channel length of 100 μm and a channel width of 200 μm. All electrical measurements were performed in ambient air at room temperature without encapsulation. The field-effect mobility was calculated in the saturation regime ($V_{DS}$ = −40 V) from the slope of the forward sweep of the measured transfer curve ($\sqrt{I_D}$ vs. $V_{GS}$), and since it varies with the gate-source voltage, it has been plotted for each data point along the transfer curve.

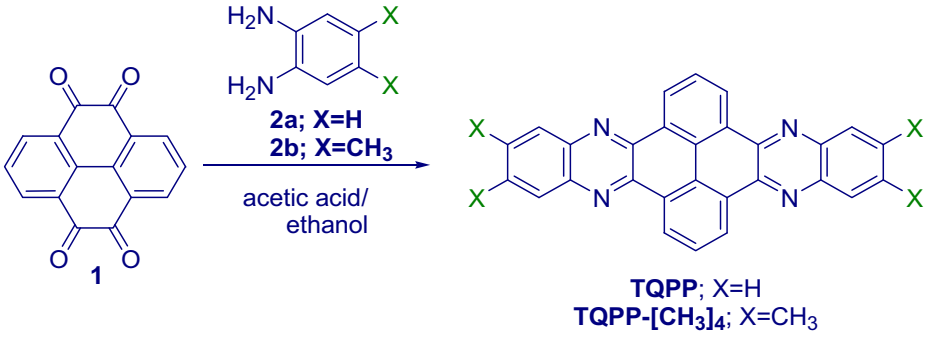


**Scheme 1.** Synthesis of the discoids **TQPP** and **TQPP-$[CH_3]_4$**.

*Scanning electron microscopy*

The thin-film morphology was imaged using a Zeiss Merlin field-emission scanning electron microscope using an acceleration voltage of 5 kV, a magnification of 50,000, and an in-lens detector.

## Results and discussion

*Synthesis*

Two discoids **TQPP** and **TQPP-[CH$_3$]$_4$** were synthesized as outlined in Scheme 1. While the structure and melting point of **TQPP** was reported by Vollmann et al. [21] no further characterization data is available for this compound in the literature. Tetraketopyrene **1** was prepared using a literature procedure [20] and was condensed with the 1,2-phenylenediamine **2a** or 4,5-dimethylphenylene-1,2-diamine **2b** (both commercially available) to yield **TQPP** and **TQPP-[CH$_3$]$_4$**, respectively. This condensation proceeded with good yields (>80%), but gave compounds with an innate insolubility in most common organic solvents. Purification was achieved by triturating the obtained solids with boiling toluene via Soxhlet extraction for 6 h followed by recrystallization from 1,2-dichlorobenzene. The low solubility made it difficult to collect $^{13}$C NMR spectra for **TQPP-[CH$_3$]$_4$** and electrochemical data on both compounds. Both, **TQPP** and **TQPP-[CH$_3$]$_4$** sublime so that electronic-grade purity was achieved.

*Thermal and spectroscopic properties*

Thermogravimetric analysis (TGA) showed the onset of weight loss (attributed to decomposition) of both compounds at approximately 370 °C under an air atmosphere. This observed stability is markedly higher in comparison to tetraazaoctacene, characterized by two additional fused phenyl units along the long axis of the molecule, which starts to decompose at 325 °C even under a nitrogen atmosphere [7]. The UV–vis spectra of **TQPP** and **TQPP-[CH$_3$]$_4$** are shown in Fig. 1. **TQPP-[CH$_3$]$_4$** showed characteristic absorption bands at 309, 326, 355, 376, 396, and 420 nm. An average 3 meV bathochromic shift is observed for the longest wavelength absorption bands. This shift is ascribed to the electron-releasing effect of the methyl groups [22] expected to lower the HOMO energy level of **TQPP-[CH$_3$]$_4$** as compared to the parent **TQPP**.

*Single crystal X-ray crystal structure analysis*

The molecular structures of **TQPP** and **TQPP-[CH$_3$]$_4$** were determined by single-crystal X-ray crystal structure analysis. The structures are shown in Supplementary data, Fig. S1. The molecules are planar with deviations from planarity in the 0.004–0.008 Å range for the individual rings in **TQPP** and 0.002–0.008 Å for **TQPP-[CH$_3$]$_4$** while the dihedral angles range from 1.11(3)–1.70(3)° and 0.96(5)–1.53(5)°, respectively, see Supplementary data, Table S4.

Single crystal X-ray crystallography was used to study the extended structures of these materials in the solid state and to determine whether the discotic-based columns are vertical or inclined. Furthermore, the nature of intermolecular interactions between the discoid mesogens and the degree of aromatic overlap between the stacking molecules can be used to gain insight into their ability of transporting charge carriers along the column axis of the stacks [23].

For **TQPP** and **TQPP-[CH$_3$]$_4$**, interplanar π-stacking distances of 3.42 Å and 3.45 Å were observed, respectively, which is well in agreement with the π–π stacking distance of 3.3–3.6 Å for TQPP-[SC$_{12}$H$_{25}$]$_4$ [19]. Packing motives of interleaved stacked sheets for

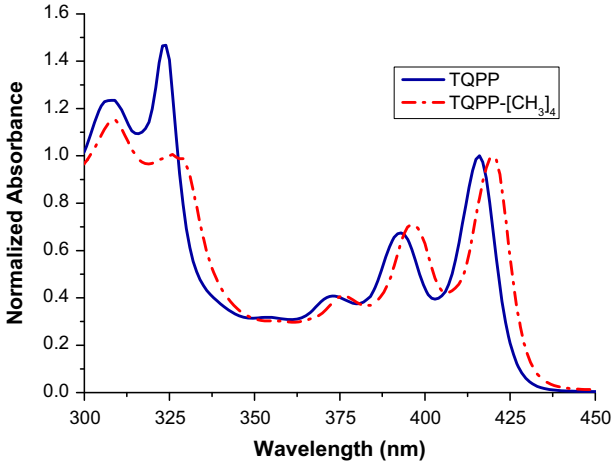


**Fig. 1.** Absorption of **TQPP** and **TQPP-[CH$_3$]$_4$** recorded in 1,2-dichlorobenzene.

**TQPP** Fig. 2 (left) and stacked sheets for **TQPP-[CH$_3$]$_4$** Fig. 2 (right) were observed.

*SEM of thin films*

The thin-film morphology of vacuum-deposited films of the two semiconductors appears similar when studied by scanning electron microscopy. Only subtle differences are noted, e.g., in the grain size (i.e., the grains in the **TQPP** films appear to be larger than in **TQPP-[CH$_3$]$_4$**), Fig. 3.

*Theoretical calculations*

Device performance is fundamentally influenced by the charge carrier mobility. The mobility is influenced by factors such as molecular packing, disorder, and impurities to name a few. Hence, theoretical calculations were carried out to estimate the key charge transport parameters of **TQPP** and **TQPP-[CH$_3$]$_4$**. A top view of the (columnar) structures and of the couplings between the molecules is displayed in Figs. 4 and 5, respectively.

The charge transfer rate between two adjacent molecules $k_{12}$ can be expressed in first approximation in the hopping regime within the semi-classical Marcus formalism as Eq. (1): [24]

$$k_{12} = \frac{2\pi}{\hbar}|t_{12}|^2 \frac{1}{\sqrt{4\pi\lambda k_B T}} e^{-\frac{(\Delta G^\circ + \lambda)^2}{4\lambda k_B T}} \quad (1)$$

- $\lambda$ is the total reorganization energy, which reflects the changes in the geometry of the molecules and the changes in the electronic and nuclear polarization of the medium between the initial and final states.
- $\Delta G^\circ$ is the free enthalpy of the reaction, whose value is zero for a self-exchange process, in the absence of an electric field.
- $t_{12}$ is the electronic coupling between the initial and final states.

The simplest approach to calculate the transfer integral (i.e., electronic coupling) is to estimate it as half the splitting of the HOMO [LUMO] levels in a neutral dimer for hole [electron] transport [25]. However, for non-centrosymmetric structures, this approach is often biased by electrostatic effects, which create an initial offset of the electronic levels before they start to interact. This offset does not contribute to the transfer efficiency. In line with our recent theoretical works, we calculated the transfer integral values directly using a fragment approach at the Density Functional Theory (DFT) level using the B3LYP functional with a

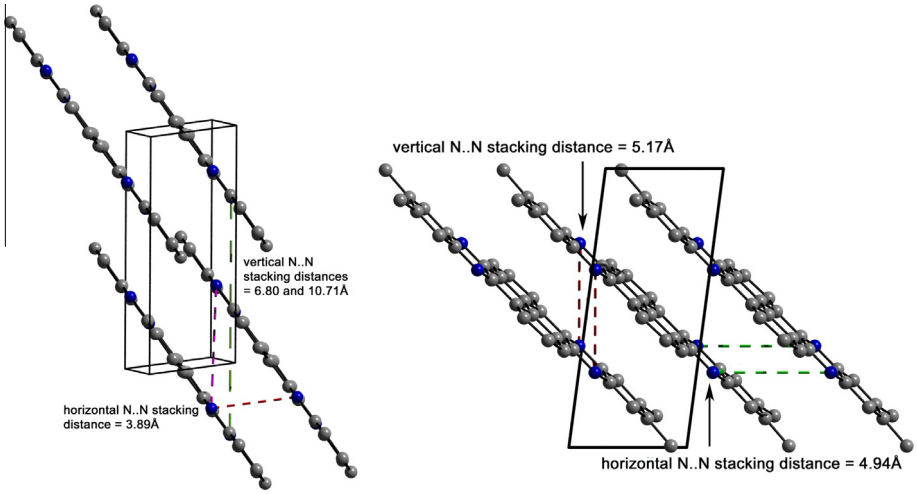


**Fig. 2.** π-Stacking distances for **TQPP** (left) and **TQPP-[CH$_3$]$_4$** (right). The N. . .N interplanar distances are indicated in the figures.

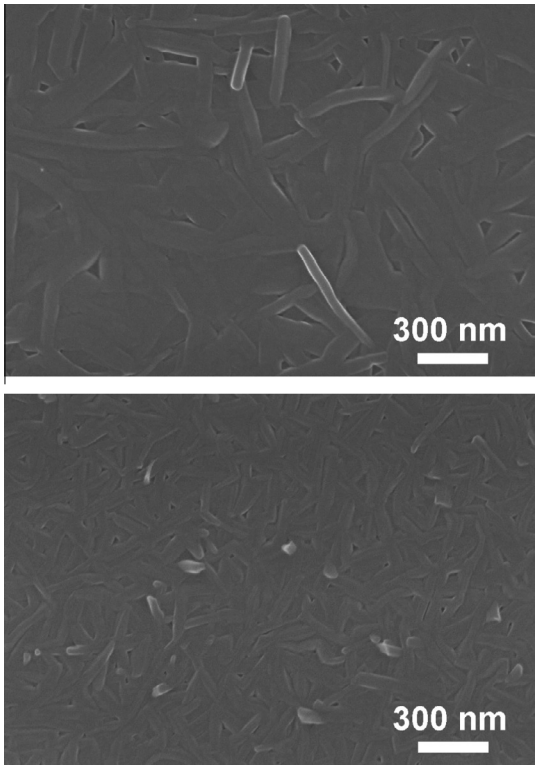


**Fig. 3.** Scanning electron microscopy images of 30-nm-thick films of the semiconductors **TQPP** (top) and **TQPP-[CH$_3$]$_4$** (bottom), vacuum-deposited onto Si/SiO$_2$/Al$_2$O$_3$/SAM substrates.

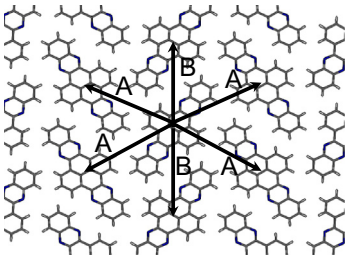


**Fig. 4.** Inter-columnar coupling paths for TQPP.

triple zeta polarized (TZP) basis set within the Amsterdam Density Functional (ADF) package [26].

The estimated internal reorganization energies (at the DFT B3LYP/6-31G** level) [27] for **TQPP** and **TQPP-[CH$_3$]$_4$** are attractive compared to compounds with high charge mobilities such as oligoacenes, see Table 1.

We have next calculated the electronic coupling between molecules in the same column (intra) which is expected to be the largest. This yields values of 62.4 meV and 14.5 meV for holes and electrons, respectively, in **TQPP** while values of 8.6 meV and 18.6 meV are obtained for **TQPP-[CH$_3$]$_4$**. In contrast, the electronic coupling in tetracene, pentacene, and rubrene are on the order of 70, 85, and 83 meV, respectively [29].

We have also estimated the electronic couplings for the major inter-columnar paths that are represented in Figs. 4 and 5. Note that for each path (A, B, C), the charge can be transferred either to the molecule in the plane located above that of the initial site or to a molecule in the lower plane (i.e., to the two closest neighbors), Table 2. This leads to two possible jumps along each path (A and A′ for example). The results show that the transport is mostly one-dimensional for holes in **TQPP** since the electronic

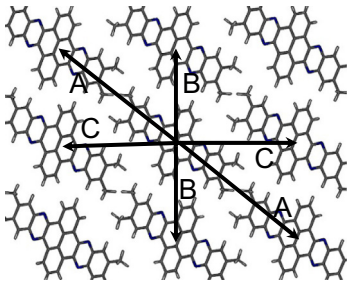


**Fig. 5.** Inter-columnar coupling paths for TQPP-[CH$_3$]$_4$.

**Table 1**
Calculated internal reorganization energies of discoids **TQPP** and **TQPP-[CH$_3$]$_4$** in comparison to representative acenes.

| | TQPP | TQPP-[CH$_3$]$_4$ | Tetracene [28] | Anthracene [28] | Pentacene [28] |
|---|---|---|---|---|---|
| $\lambda_i$ (holes), eV | 0.118 | 0.114 | 0.113 | 0.137 | 0.097 |
| $\lambda_i$ (electrons), eV | 0.080 | 0.085 | 0.160 | 0.196 | 0.132 |

**Table 2**
Electronic coupling of **TQPP** and **TQPP-[CH$_3$]$_4$** for the different paths.

| | | Electronic coupling (cm$^{-1}$) | |
|---|---|---|---|
| | | HOMO | LUMO |
| TQPP | Intra | 503 | 117 |
| | A | 2 | 1 |
| | A′ | 9 | 10 |
| | B | 43 | 1 |
| | B′ | 120 | 69 |
| TQPP-[CH$_3$]$_4$ | Intra | 69 | 150 |
| | A | 29 | 29 |
| | A′ | 56 | 34 |
| | B | 1 | 31 |
| | B′ | 11 | 10 |
| | C | 2 | 2 |
| | C′ | 17 | 23 |

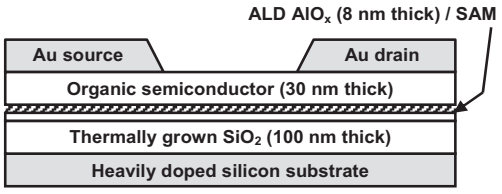


**Fig. 6.** Schematic cross-section of the fabricated OTFTs.

**Table 3**
Performance of **TQPP** and **TQPP-(CH$_3$)$_4$** in bottom-gate OTFTs in air.

| Compound | Field-effect mobility (cm$^2$/V s) | On/Off ratio | Subthreshold swing (V/decade) |
|---|---|---|---|
| TQPP | 0.0025 | $10^4$ | 3.6 |
| TQPP-(CH$_3$)$_4$ | $7 \times 10^{-5}$ | $10^2$ | 3.4 |

coupling largely dominates between adjacent molecules lying in the same column. In contrast, a two-dimensional character prevails for holes in **TQPP-[CH$_3$]$_4$** where inter-columnar and intra-columnar hopping processes appear to be similarly efficient.

*Performance in OTFT device geometry*

In order to evaluate the potential of the new organic semiconductors for electronic applications experimentally, organic thin-film transistors (OTFTs) in a bottom-gate, top-contact device structure were fabricated and characterized; see Fig. 6 and Table 3.

The electrical measurements show that the charge-carrier mobility in thin films of **TQPP** is a factor of 35 larger than the charge-carrier mobility in thin films of **TQPP-[CH$_3$]$_4$**, Fig. 7. This illustrates the significant impact on the charge transport as created by the methyl groups at the periphery of the molecule. The semiconductor without any substitution, **TQPP,** gives the larger mobility (0.0025 cm$^2$/V s) whilst a mobility of $7 \times 10^{-5}$ cm$^2$/V s is found in the methyl-substituted semiconductor **TQPP-[CH$_3$]$_4$**.

Among others, possible origins for the observed differences include different orientation of the molecules with respect to the substrate surface, grain size as well as charge transfer rates as evidenced by electronic coupling. As was observed by SEM, Fig. 3, the methyl substitution has a large effect on the morphology of the semiconductor films. In particular, the size and orientation of the crystalline regions and the density of grain boundaries among others are effected [30,31].

In addition, the observed difference in mobilities may substantially also be rationalized by our computational simulations. According to Eq. (1), the mobilities scale with the square of the electronic coupling [32]. Indeed, the highest electronic coupling for **TQPP-[CH$_3$]$_4$** is 69 cm$^{-1}$, a very low value compared to electronic couplings computed for **TQPP** (503 cm$^{-1}$ along the stacks, and a value of 120 cm$^{-1}$ for one inter-columnar coupling). Hence, the ratio between the intra-columnar couplings (~7) is consistent with the ratio between mobilities (~35).

## Conclusions

In summary, both **TQPP** and **TQPP-[CH$_3$]$_4$** exhibit p-type semiconducting properties. Particularly, **TQPP** exhibits more favorable hole transport properties compared to **TQPP-[CH$_3$]$_4$** in OFET geometry. Based on computational calculations, the electronic

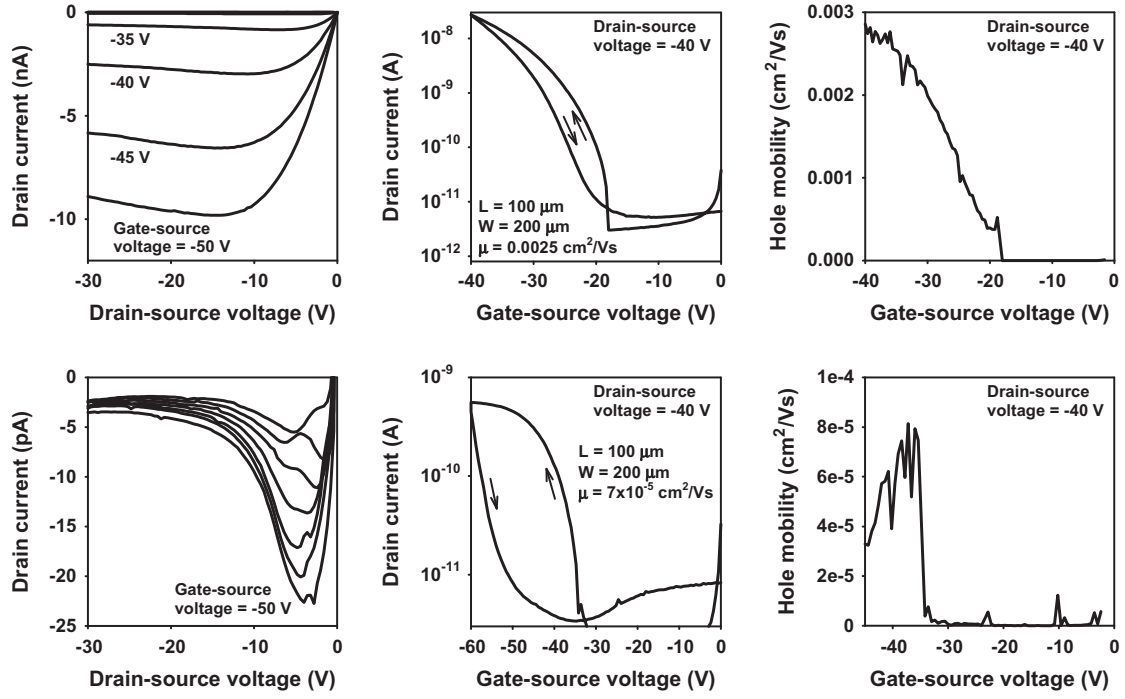


**Fig. 7.** Measured output ($I_D$ vs. $V_{DS}$) and transfer ($I_D$ vs. $V_{GS}$) characteristics of the OTFTs based on **TQPP** (top) and **TQPP-[CH$_3$]$_4$** (bottom) in air.

couplings are larger for **TQPP** than for **TQPP-[$CH_3$]$_4$**, especially for intra-columnar couplings. Inter-columnar couplings differ less among the two systems. **TQPP** shows mostly one-dimensional hole transport, while **TQPP-[$CH_3$]$_4$** transports holes almost equally along two directions (2D transport).

## Acknowledgements

This work was supported by the Lebanese National Council for Scientific Research (CNRS), the Petroleum Research Fund (PRF) of the American Chemical Society (Grant No. 47343-B10), and the Royal Society of Chemistry. The authors are grateful for this support. Crystallographic data were collected through the SCrALS (Service Crystallography at Advanced Light Source) program at Beamline 11.3.1 at the Advanced Light Source (ALS), Lawrence Berkeley National Laboratory (supported by the U.S. Department of Energy, Office of Basic Energy Sciences, under contract No. DE-AC02-05CH11231). The work in Mons is supported by the Interuniversity Attraction Pole Programs of the Belgian Federal Science Policy Office (PAI 7/05) and by the Belgian National Fund for Scientific Research (FNRS). J. C. is an FNRS Research Director. B.W. and B. R. K. thank the Arab Fund Fellowship Program for financial support.

## Appendix A. Supplementary material

Experimental parameters and data tables for X-ray crystallography of **TQPP** and **TQPP-[$CH_3$]$_4$** are available online at http://www.sciencedirect.com. CCDC 1022119 – 1022120 contain the supplementary crystallographic data for this paper. These data can be obtained free of charge from The Cambridge Crystallographic Data Centre via www.ccdc.cam.ac.uk/data_request/cif. Supplementary data associated with this article can be found, in the online version, at http://dx.doi.org/10.1016/j.molstruc.2015.03.057. These data include MOL files and InChiKeys of the most important compounds described in this article.

## References

[1] J. Hu, D. Zhang, S. Jin, S.Z.D. Cheng, F.W. Harris, Chem. Mater. 16 (2004) 4912–4915.
[2] S.W. Leng, L.H. Chan, J.K. Jing, J. Hu, R.M. Moustafa, R.M. Van Horn, M.J. Graham, B. Sun, M.F. Zhu, K.U. Jeong, B.R. Kaafarani, W.B. Zhang, F.W. Harris, S.Z.D. Cheng, Soft Matter 6 (2010) 100–112.
[3] D.C. Lee, K.K. McGrath, K. Jang, Chem. Commun. (2008) 3636–3638.
[4] K.K. McGrath, K. Jang, K.A. Robins, D.C. Lee, Chem. – Eur. J. 15 (2009) 4070–4077.
[5] J. Li, P. Li, J. Wu, J. Gao, W.-W. Xiong, G. Zhang, Y. Zhao, Q. Zhang, J. Org. Chem. 79 (2014) 4438–4445.
[6] G. Li, A.P. Abiyasa, J. Gao, Y. Divayana, W. Chen, Y. Zhao, X.W. Sun, Q. Zhang, J. Org. Chem. 1 (2012) 346–351.
[7] A. Mateo-Alonso, N. Kulisic, G. Valenti, M. Marcaccio, F. Paolucci, M. Prato, Chem. – Asian J. 5 (2010) 482–485.
[8] S. More, R. Bhosale, S. Choudhary, A. Mateo-Alonso, Org. Lett. 14 (2012) 4170–4173.
[9] S. More, S. Choudhary, A. Higelin, I. Krossing, M. Melle-Franco, A. Mateo-Alonso, Chem. Commun. 50 (2014) 1976–1979.
[10] B. Gao, M. Wang, Y. Cheng, L. Wang, X. Jing, F. Wang, J. Am. Chem. Soc. 130 (2008) 8297–8306.
[11] C. Tong, W. Zhao, J. Luo, H. Mao, W. Chen, H.S.O. Chan, C. Chi, Org. Lett. 14 (2012) 494–497.
[12] U.H.F. Bunz, Chem. – Eur. J. 15 (2009) 6780–6789.
[13] U.H.F. Bunz, Pure Appl. Chem. 82 (2010) 953–968.
[14] U.H.F. Bunz, J.U. Engelhart, B.D. Lindner, M. Schaffroth, Angew. Chem. 52 (2013) 3810–3821.
[15] M. Winkler, K.N. Houk, J. Am. Chem. Soc. 129 (2007) 1805–1815.
[16] A. Mateo-Alonso, Chem. Soc. Rev. 43 (2014) 6311–6324.
[17] S. More, R. Bhosale, A. Mateo-Alonso, Chem. – Eur. J. 20 (2014) 10626–10631.
[18] B.R. Kaafarani, L.A. Lucas, B. Wex, G.E. Jabbour, Tetrahedron Lett. 48 (2007) 5995–5998.
[19] L.A. Lucas, D.M. DeLongchamp, L.J. Richter, R.J. Kline, D.A. Fischer, B.R. Kaafarani, G.E. Jabbour, Chem. Mater. 20 (2008) 5743–5749.
[20] J. Hu, D. Zhang, F.W. Harris, J. Org. Chem. 70 (2005) 707–708.
[21] H. Vollmann, H. Becker, M. Corell, H. Streeck, Chemie 531 (1937) 1–159.
[22] B.D. Koepnick, J.S. Lipscomb, D.K. Taylor, J. Phys. Chem. A 114 (2010) 13228–13233.
[23] T.L. Andresen, F.C. Krebs, N. Thorup, K. Bechgaard, Chem. Mater. 12 (2000) 2428–2433.
[24] R.A. Marcus, J. Chem. Phys. 43 (1965) 679–701.
[25] G. Pourtois, D. Beljonne, J. Cornil, M.A. Ratner, J.L. Brédas, J. Am. Chem. Soc. 124 (2002) 4436–4447.
[26] L. Viani, Y. Olivier, S. Athanasopoulos, D.A. da Silva, J. Hulliger, J.L. Brédas, J. Gierschner, J. Cornil, ChemPhysChem 11 (2010) 1062–1068.
[27] A. Van Vooren, J.S. Kim, J. Cornil, ChemPhysChem 9 (2008) 989–993.
[28] V. Coropceanu, M. Malagoli, D.A. da Silva, N.E. Gruhn, T.G. Bill, J.L. Brédas, Phys. Rev. Lett. 89 (2002).
[29] V. Coropceanu, J. Cornil, D.A. da Silva, Y. Olivier, R. Silbey, J.L. Brédas, Chem. Rev. 107 (2007). 2165-2165.
[30] H. Sirringhaus, Adv. Mater. 26 (2014) 1319–1335.
[31] C.-A. Di, Y. Liu, G. Yu, D. Zhu, Acc. Chem. Res. 42 (2009) 1573–1583.
[32] V. Lemaur, D.A. Da Silva Filho, V. Coropceanu, M. Lehmann, Y. Geerts, J. Piris, M.G. Debije, A.M. Van de Craats, K. Senthilkumar, L.D.A. Siebbeles, J.M. Warman, J.L. Brédas, J. Cornil, J. Am. Chem. Soc. 126 (2004) 3271–3279.